

## Spin Relaxation in Single-Layer and Bilayer Graphene

Wei Han and R. K. Kawakami\*

*Department of Physics and Astronomy, University of California, Riverside, California 92521, USA*

(Received 1 February 2011; published 21 July 2011)

We investigate spin relaxation in graphene spin valves and observe strongly contrasting behavior for single-layer graphene (SLG) and bilayer graphene (BLG). In SLG, the spin lifetime ( $\tau_s$ ) varies linearly with the momentum scattering time ( $\tau_p$ ) as carrier concentration is varied, indicating the dominance of Elliot-Yafet (EY) spin relaxation at low temperatures. In BLG,  $\tau_s$  and  $\tau_p$  exhibit an inverse dependence, which indicates the dominance of Dyakonov-Perel spin relaxation at low temperatures. The different behavior is due to enhanced screening and/or reduced surface sensitivity of BLG, which greatly reduces the impurity-induced EY spin relaxation.

DOI: 10.1103/PhysRevLett.107.047207

PACS numbers: 85.75.-d, 72.25.Rb, 81.05.ue

Graphene is an attractive material for spintronics due to the possibility of long spin lifetimes arising from low intrinsic spin-orbit coupling and weak hyperfine coupling [1–5]. However, Hanle spin precession experiments in graphene spin valves report spin lifetimes that are orders of magnitude shorter than expected theoretically [6–12]. This has prompted theoretical studies of the extrinsic sources of spin relaxation such as impurity scattering [13], ripples [5], and substrate effects [14]. Experimentally, several studies have investigated spin relaxation including the roles of impurity scattering [7,11] and graphene thickness [15]. Recently, it has been shown that ferromagnet (FM) contact-induced spin relaxation is responsible for the short spin lifetimes observed in experiments [12]. Therefore, high quality tunneling contacts are necessary to suppress the contact-induced effects for systematic investigations of spin relaxation in graphene.

In this Letter, we perform systematic studies of spin relaxation in single-layer graphene (SLG) and bilayer graphene (BLG) spin valves with tunneling contacts. The dependence of spin lifetime on temperature and carrier concentration (tuned by gate voltage) reveals rather different spin relaxation mechanisms in the two systems. In SLG, the temperature dependence shows similar trends of the spin lifetime and momentum scattering time, and the low temperature gate voltage dependence shows a strong linear scaling of the two quantities. This indicates the dominance of Elliot-Yafet (EY) spin relaxation, which most likely comes from impurity scattering. In BLG, the temperature dependence and low temperature gate voltage dependence show a nearly inverse relationship between the spin lifetime and momentum scattering time. This indicates the dominance of Dyakonov-Perel (DP) spin relaxation, which can be generated by ripples in the graphene. The contrasting behaviors of SLG and BLG can be understood as a reduction of the impurity scattering in BLG due to the enhanced screening of the impurity potential and reduced surface sensitivity. This leads to longer spin lifetimes ( $\sim 6.2$  ns, the highest value observed in graphene

spin valves to date) and the greater role of DP spin relaxation observed in BLG.

The graphene flakes are mechanically exfoliated from highly oriented pyrolytic graphite onto an SiO<sub>2</sub> (300 nm thickness)/Si substrate [16]. Gate voltage is applied to the Si substrate to tune the carrier concentration in graphene. SLG and BLG are identified by optical microscopy and Raman spectroscopy [17]. Standard *e*-beam lithography with PMMA/MMA bilayer resist is used to define the Au and Co electrodes. First, two Au electrodes are put down on the two ends of the graphene. Then a second step of *e*-beam lithography is used for the Co electrodes, where subsequent angle evaporations of TiO<sub>2</sub>, MgO, and Co produce the ferromagnetic electrodes with tunneling contacts [12,18].

Studies of spin transport and spin relaxation are performed on graphene spin valves consisting of two spin-sensitive Co electrodes (E2, E3) and two Au electrodes (E1, E4). Nonlocal voltages ( $V_{NL}$ ) are measured using lock-in detection with an ac injection current of  $I = 1 \mu\text{A rms}$  at 13 Hz [18]. The nonlocal resistance ( $R_{NL} = V_{NL}/I$ ) is measured as a function of in-plane magnetic field [Fig. 1(a) inset] to detect the spin injection and transport [6,19–24]. Figure 1(a) shows the nonlocal magnetoresistance (MR) curves for a typical SLG device (device A) at the charge neutrality point (CNP). The nonlocal MR ( $\Delta R_{NL}$ ) is indicated by the red or gray arrow, which is the magnitude of the sharp change in  $R_{NL}$ .

The spin lifetime ( $\tau_s$ ), diffusion coefficient ( $D$ ), and spin diffusion length ( $\lambda = \sqrt{D\tau_s}$ ) are determined by the Hanle spin precession measurement [Fig. 1(b) inset] [20]. Applying an out-of-plane magnetic field ( $H_{\perp}$ ) causes the spins to precess as they diffuse from E2 to E3, which results in characteristic Hanle curves as shown for device A at 300 K [Fig. 1(b)]. The red or gray circles (black circles) are for the parallel (antiparallel) alignment of the Co magnetizations.  $\tau_s$  and  $D$  are determined by fitting the Hanle curves with

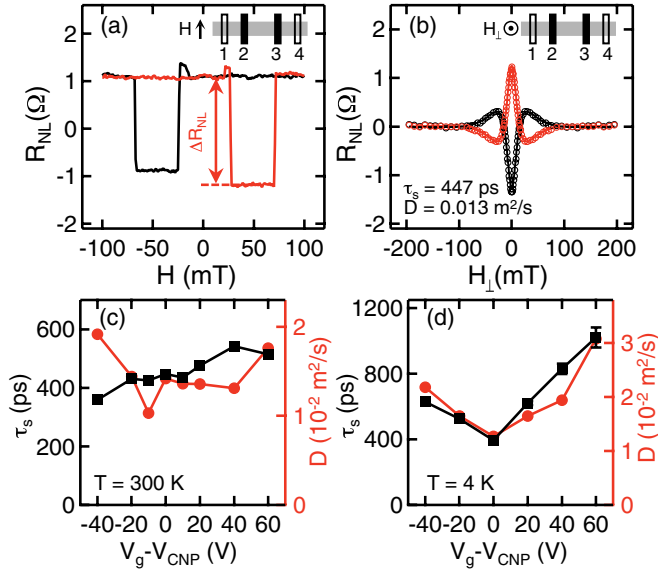


FIG. 1 (color online). (a) Nonlocal MR measurement of device A (SLG) at 300 K. The red or gray (black) curve is measured as the field is swept up (down). E1 and E4 are Au electrodes (labeled 1 and 2), and E2 and E3 are Co electrodes (labeled 2 and 3). (b) Hanle measurements of device A at 300 K. The red or gray (black) circles are data taken for parallel (antiparallel) Co magnetizations. The solid lines are the best fit by Eq. (1). (c), (d) Spin lifetime (squares) and diffusion coefficient (circles) as a function of gate voltage at 300 and 4 K, respectively.

$$R_{NL} \propto \pm \int_0^\infty \frac{1}{\sqrt{4\pi Dt}} \exp\left[-\frac{L^2}{4Dt}\right] \cos(\omega_L t) \times \exp(-t/\tau_s) dt \quad (1)$$

where the  $+$  ( $-$ ) sign is for the parallel (antiparallel) magnetization state,  $L$  is the spacing between the Co electrodes,  $\omega_L = g\mu_B H_\perp / \hbar$  is the Larmor frequency,  $g$  is the  $g$  factor,  $\mu_B$  is the Bohr magneton, and  $\hbar$  is the reduced Planck's constant. For device A,  $D = 0.013 \text{ m}^2/\text{s}$ ,  $\tau_s = 447 \text{ ps}$ , and  $\lambda = 2.4 \text{ } \mu\text{m}$ . The  $\tau_s$  and  $D$  obtained from the Hanle curves are plotted as a function of gate voltage in Figs. 1(c) and 1(d) for 300 and 4 K, respectively. At 300 K, there is no obvious correlation between  $\tau_s$  and  $D$ . Interestingly, when the device is cooled to  $T = 4 \text{ K}$ ,  $\tau_s$  and  $D$  exhibit a strong correlation, with both quantities increasing with carrier concentration. The correlation of  $\tau_s$  and  $D$  implies a linear relation between  $\tau_s$  and the momentum scattering time,  $\tau_p$  ( $D \sim \tau_p$  as discussed in Refs. [7, 15, 25]). This indicates that at low temperatures the spin scattering is dominated by momentum scattering through the EY mechanism (i.e., finite probability of a spin-flip during a momentum scattering event) [26–28]. This behavior has been observed in five SLG devices (mobility: 1000–3000  $\text{cm}^2/\text{Vs}$ ).

The temperature dependences of  $\tau_s$  and  $D$  at different carrier concentrations are shown in Figs. 2(a) and 2(b). As the temperature decreases from 300 to 4 K,  $\tau_s$  shows a

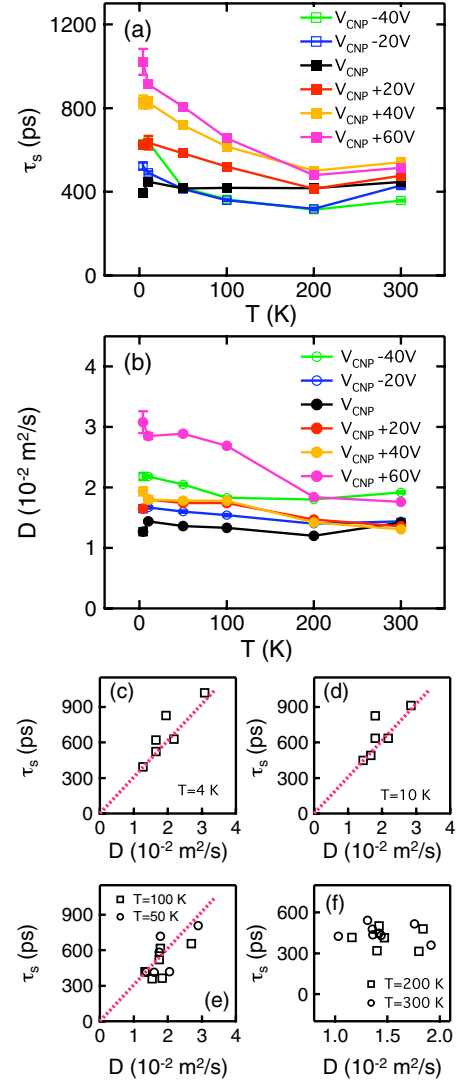


FIG. 2 (color online). Temperature dependence of SLG spin valves (device A). (a),(b) Temperature dependence of spin lifetime and diffusion coefficient at different gate voltages relative to the charge neutrality point. (c)–(f) Plot of spin lifetime vs diffusion coefficient at  $T = 4 \text{ K}$ ,  $T = 10 \text{ K}$ ,  $T = 50 \text{ K}$  and  $100 \text{ K}$ ,  $T = 200 \text{ K}$ , and  $300 \text{ K}$ , respectively. The dotted line is a linear fit of the spin lifetime vs diffusion coefficient.

modest increase at higher carrier densities (e.g., from  $\sim 0.5 \text{ ns}$  to  $\sim 1 \text{ ns}$  for  $V_g - V_{\text{CNP}} = +60 \text{ V}$ ) and little variation for lower carrier densities. The temperature dependence of  $D$  shows a similar behavior as  $\tau_s$ . To analyze the relationship between the spin scattering and momentum scattering, we plot  $\tau_s$  vs  $D$  for temperatures  $T = 4 \text{ K}$  [Fig. 2(c)],  $T = 10 \text{ K}$  [Fig. 2(d)],  $T = 50$  and  $100 \text{ K}$  [Fig. 2(e)],  $T = 200$  and  $300 \text{ K}$  [Fig. 2(f)], respectively. The main trend is that for lower temperatures,  $\tau_s$  scales linearly with  $D$ , which indicates that an EY spin relaxation mechanism is dominant at lower temperatures ( $\leq 100 \text{ K}$ ). For higher temperatures,  $\tau_s$  and  $D$  do not follow the linear relationship as shown at low temperatures, which

suggests that multiple sources of spin scattering are present.

Next, we investigate spin relaxation in BLG spin valves, which differs from SLG not just in thickness but also in band structure (linear for SLG, parabolic for BLG) and intrinsic spin-orbit coupling [29,30]. Figure 3(a) shows the

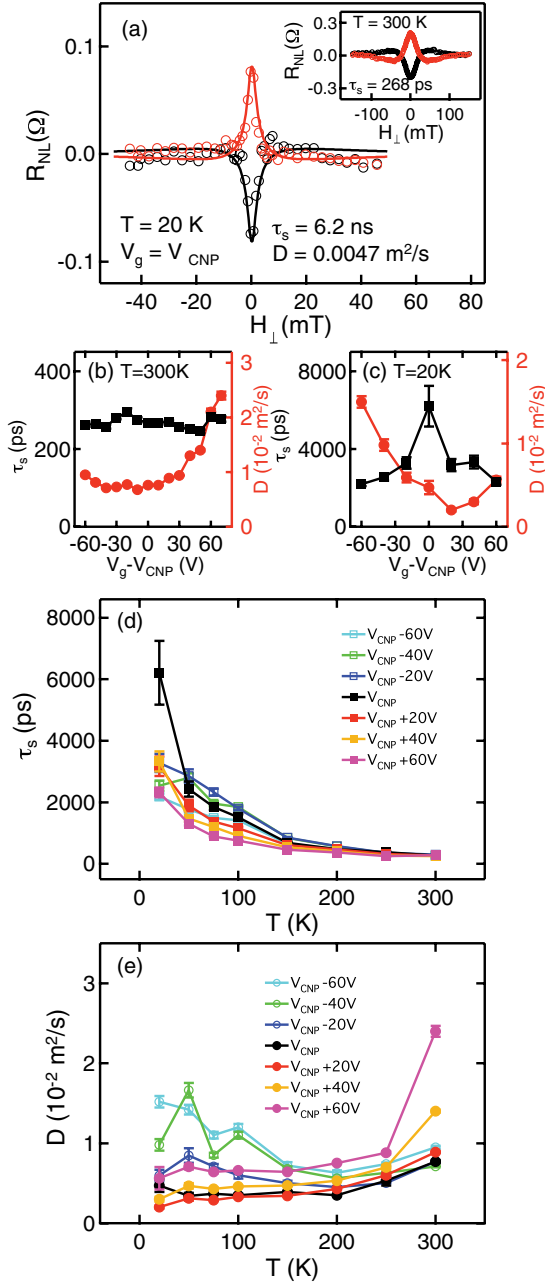


FIG. 3 (color online). Gate and temperature dependence of BLG spin valves (device B). (a) Hanle measurement at 20 K for  $V_g = V_{CNP}$ . Inset: Hanle measurement at 300 K for  $V_g = V_{CNP}$ . (b),(c) Spin lifetime (squares) and diffusion coefficient (circles) as a function of gate voltage at 300 and 20 K. (d), (e) Temperature dependence of spin lifetime and diffusion coefficient at different gate voltages relative to the charge neutrality point.

Hanle curve of the longest observed spin lifetime of 6.2 ns, which is obtained on device B for CNP at 20 K. Figure 3(a) inset shows the Hanle curve at 300 K with best fit parameter of  $\tau_s = 268$  ps. The gate voltage dependences of  $\tau_s$  and  $D$  at 300 K and 20 K are shown in Figs. 3(b) and 3(c), respectively. At 300 K,  $\tau_s$  varies from 250 to 300 ps as a function of gate voltage and exhibits no obvious correlation with  $D$ . At 20 K,  $\tau_s$  varies from 2.5 to 6.2 ns, showing a peak at the charge neutrality point. On the other hand, the gate voltage dependence of  $D$  exhibits lower values near the charge neutrality point and increasing values at higher carrier densities. The opposite behaviors of  $\tau_s$  and  $D$  suggest the importance of DP spin relaxation (i.e., spin relaxation via precession in internal spin-orbit fields) where  $\tau_s$  scales inversely with  $\tau_p$  [28,31]. This behavior has been observed in four BLG devices (mobility: 400–1300 cm<sup>2</sup>/V s). Figures 3(d) and 3(e) show the temperature dependences of  $\tau_s$  and  $D$ , respectively. The opposite trends of the temperature dependences of  $\tau_s$  and  $D$  suggest the strong contributions of spin relaxation mechanisms of the DP type, which is also suggested in Ref. [32].

To investigate the spin relaxation in BLG quantitatively, we perform a detailed measurement of the gate voltage dependence of a BLG spin valve (device C) at 4 K. In Fig. 4(a),  $\tau_s$  and  $D$  exhibit opposite dependences as a function of gate voltage, indicating the importance of DP spin relaxation. Quantitatively, the spin relaxation rate could be expressed as

$$\frac{1}{\tau_s} = \frac{1}{\tau_s^{EY}} + \frac{1}{\tau_s^{DP}} = \frac{K_{EY}}{D} + K_{DP}D \quad (2)$$

Figure 4(b) shows the spin relaxation rate ( $1/\tau_s$ ) as a function of  $D$  for BLG (device C at 4 K). The best fit by Eq. (2) yields  $K_{EY} = 0.05 \pm 0.01$  (10<sup>-2</sup> m<sup>2</sup> s<sup>-1</sup>) ns<sup>-1</sup>, and  $K_{DP} = 1.24 \pm 0.09$  (10<sup>-2</sup> m<sup>2</sup> s<sup>-1</sup>)<sup>-1</sup> ns<sup>-1</sup>. The contributions from EY and DP spin relaxation are shown by the dashed lines. For the experimental range of  $D$ , the DP contribution to spin relaxation is much stronger than the EY contribution. For comparison, we plot the spin relaxation rate as a function of  $D$  [Fig. 4(b) inset] for SLG (device A at 4 K). The best fit parameters are  $K_{EY} = 3.05 \pm 0.35$  (10<sup>-2</sup> m<sup>2</sup> s<sup>-1</sup>) ns<sup>-1</sup>, and  $K_{DP} = -0.02 \pm 0.10$  (10<sup>-2</sup> m<sup>2</sup> s<sup>-1</sup>)<sup>-1</sup> ns<sup>-1</sup>, which is zero within the error bars.

Possible sources of extrinsic EY spin relaxation include long-range (Coulomb) impurity scattering and short-range impurity scattering [13], while an extrinsic DP spin relaxation could arise from curvature of the graphene film [1,5]. The transition from EY-dominated SLG to the DP-dominated BLG could be due to a strong reduction of the EY contribution because of enhanced screening of the impurity potential in thicker graphene [15,33] and the smaller surface-to-volume ratio. However, a quantitative explanation for the substantial differences in spin relaxation between SLG and BLG will require further theoretical and experimental studies. Specifically, understanding the relationship

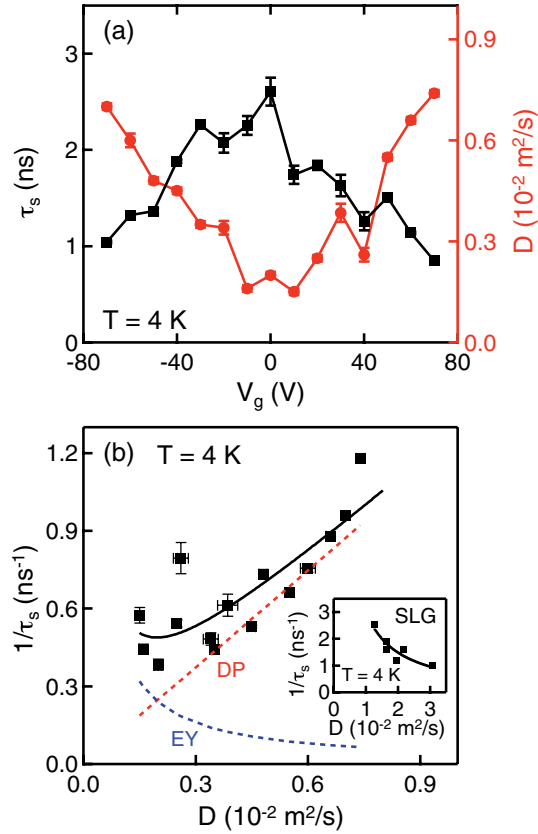


FIG. 4 (color online). Gate voltage dependence of BLG spin valves (device C). (a) Spin lifetime (squares) and diffusion coefficient (circles) as a function of gate voltage at 4 K. (b) Spin relaxation rate as a function of diffusion coefficient. The black solid line is the best fit based on Eq. (2). Inset: Spin relaxation rate as a function of diffusion coefficient for SLG (device A) at 4 K with the best fit (solid line) based on Eq. (2).

between spin relaxation and the characteristics that differentiate SLG from BLG (e.g., band structure, lattice symmetry, band gap formation in BLG, etc.) may be essential. For example, it has been shown by Dugaev *et al.* that in the presence of random spin-orbit interactions (which could be produced by curvature domains), the DP-like contribution to the spin lifetime has different values and decreases more rapidly with carrier concentration for massive fermions (BLG case) than for massless fermions (SLG case) [34,35], even with the same spin-orbit coupling strength.

In summary, long spin lifetimes are observed in both SLG and BLG. Furthermore, temperature and gate dependences of the spin lifetime and diffusion coefficient reveal the contrasting behavior of SLG and BLG, in which EY spin scattering dominates in SLG, while DP spin relaxation dominates in BLG.

We acknowledge technical assistance and discussion with E. Sherman, K. M. McCreary, H. Wen, J. J. I. Wong, A. G. Swartz, K. Pi, and Y. Li and the support of ONR

(N00014-09-1-0117), NSF (DMR-1007057), and NSF (MRSEC DMR-0820414).

\*roland.kawakami@ucr.edu

- [1] D. Huertas-Hernando, F. Guinea, and A. Brataas, *Phys. Rev. B* **74**, 155426 (2006).
- [2] H. Min *et al.*, *Phys. Rev. B* **74**, 165310 (2006).
- [3] Y. Yao *et al.*, *Phys. Rev. B* **75**, 041401(R) (2007).
- [4] B. Trauzettel *et al.*, *Nature Phys.* **3**, 192 (2007).
- [5] D. Huertas-Hernando, F. Guinea, and A. Brataas, *Phys. Rev. Lett.* **103**, 146801 (2009).
- [6] N. Tombros *et al.*, *Nature (London)* **448**, 571 (2007).
- [7] C. Józsa *et al.*, *Phys. Rev. B* **80**, 241403(R) (2009).
- [8] M. Popinciuc *et al.*, *Phys. Rev. B* **80**, 214427 (2009).
- [9] M. Shiraishi *et al.*, *Adv. Funct. Mater.* **19**, 3711 (2009).
- [10] W. Han *et al.*, *Appl. Phys. Lett.* **94**, 222109 (2009).
- [11] K. Pi *et al.*, *Phys. Rev. Lett.* **104**, 187201 (2010).
- [12] W. Han *et al.*, *Phys. Rev. Lett.* **105**, 167202 (2010).
- [13] A. H. Castro Neto and F. Guinea, *Phys. Rev. Lett.* **103**, 026804 (2009).
- [14] C. Ertler *et al.*, *Phys. Rev. B* **80**, 041405(R) (2009).
- [15] T. Maassen *et al.*, *Phys. Rev. B* **83**, 115410 (2011).
- [16] K. S. Novoselov *et al.*, *Science* **306**, 666 (2004).
- [17] A. C. Ferrari *et al.*, *Phys. Rev. Lett.* **97**, 187401 (2006).
- [18] See supplemental material at <http://link.aps.org/supplemental/10.1103/PhysRevLett.107.047207> for detailed descriptions.
- [19] M. Johnson and R. H. Silsbee, *Phys. Rev. Lett.* **55**, 1790 (1985).
- [20] F. J. Jedema *et al.*, *Nature (London)* **416**, 713 (2002).
- [21] X. Lou *et al.*, *Nature Phys.* **3**, 197 (2007).
- [22] S. Cho, Y.-F. Chen, and M. S. Fuhrer, *Appl. Phys. Lett.* **91**, 123105 (2007).
- [23] W. Han *et al.*, *Phys. Rev. Lett.* **102**, 137205 (2009).
- [24] H. Goto *et al.*, *Appl. Phys. Lett.* **92**, 212110 (2008).
- [25] J. Fabian *et al.*, *Acta Phys. Slovaca* **57**, 565 (2007).
- [26] R. J. Elliott, *Phys. Rev.* **96**, 266 (1954).
- [27] Y. Yafet, in *Solid State Physics*, edited by F. Seitz and D. Turnbull (Academic Press Inc., New York, 1963), Vol. 14, p. 1.
- [28] F. Meier and B. P. Zachachrenya, *Optical Orientation, Modern Problems in Condensed Matter Science* (North-Holland, Amsterdam, 1984), Vol. 8.
- [29] A. K. Geim and K. S. Novoselov, *Nature Mater.* **6**, 183 (2007).
- [30] F. Guinea, *New J. Phys.* **12**, 083063 (2010).
- [31] M. I. D'yakonov and V. I. Perel', *Sov. Phys. Solid State* **13**, 3023 (1972).
- [32] T.-Y. Yang *et al.*, preceding Letter, *Phys. Rev. Lett.* **107**, 047206 (2011).
- [33] F. Guinea, *Phys. Rev. B* **75**, 235433 (2007).
- [34] V. K. Dugaev *et al.*, *Phys. Rev. B* **80**, 081301(R) (2009).
- [35] V. K. Dugaev, E. Y. Sherman, and J. Barnas, *Phys. Rev. B* **83**, 085306 (2011).